LES OF SPRAY COMBUSTION IN COMPRESSIBLE HIGH REYNOLDS NUMBER SWIRLING FLOWS

Vaidyanathan Sankaran*
and
Suresh Menon†
School of Aerospace Engineering,
Georgia Institute of Technology,
Atlanta, Georgia 30332,
suresh.menon@ae.gatech.edu

ABSTRACT

Large-Eddy Simulation (LES) has been used to simulate spray combustion in a gas-turbine combustor using a two-phase formulation that accounts for full two-way coupling between gas and liquid phase. Effect of heat release is also included in this study. Results show that droplets tend to accumulate in low vorticity regions. However, the vaporized fuel gets entrained by the vortices and this process enhances the combustion process. Significant modulation of the turbulence in the shear layers is observed due to the presence of both non-vaporizing and vaporizing droplets.

INTRODUCTION

Modelling of two-phase reacting flows is currently carried out using steady-state methods where only the time-averaged flow field is simulated. However, for complex flows, the turbulence models that are employed in these models are not adequate, and yield poor agreement between calculations and experiments. In the present study, we employ large-eddy simulations (LES) to study unsteady mixing and combustion in a realistic environment. The closure of the LES momentum and energy transport is based on an eddy viscosity model using a one-equation model for the subgrid kinetic energy. This approach is acceptable for momentum transport since most of the energy containing scales are resolved. However, this argument cannot readily be extended to reacting flows since combustion occurs at the molecular level, far below any resolved scale. Accurate modeling of scalar mixing (fuel and oxidizer) is critical for a realistic prediction of chemical reaction rates. Here, a sub-grid mixing and combustion model based on the Linear Eddy Model (LEM) that resolves the small-scale scalar mixing and combustion effects within the framework of a conventional LES approach (Menon *et al.*, 1993) is employed.

Earlier studies (Menon and Calhoon, 1996; Kim *et al.*, 1999; Chakravarthy and Menon, 2001) have established the ability of the present LES model. Extension to two-phase mixing layers flows was also demonstrated earlier (Pannala and Menon, 1998). The present study applies this two-phase model to spray combustion in a gas turbine combustor.

LARGE-EDDY SIMULATION MODEL

The LES equations are obtained by spatial filtering (using a low-pass filter based on the grid size $\overline{\Delta}$) the conservation equations of motion (Kim *et al.*, 1999):

$$\frac{\partial \overline{\rho}}{\partial t} + \frac{\partial \overline{\rho}\widetilde{u}_i}{\partial x_i} = \dot{\rho}_s$$

$$\frac{\partial \overline{\rho}\,\widetilde{u}_i}{\partial t} + \frac{\partial}{\partial x_j}[\overline{\rho}\widetilde{u}_i\widetilde{u}_j + \overline{p}\,\delta_{ij} - \overline{\tau}_{ij} + \tau_{ij}^{sgs}] = \dot{F}_{s,i}$$

$$\frac{\partial \overline{\rho}\widetilde{E}}{\partial t} + \frac{\partial}{\partial x_i}[(\overline{\rho}\widetilde{E} + \overline{p})\widetilde{u}_i + \overline{q}_i - \widetilde{u}_j\overline{\tau}_{ji} + H_i^{sgs} + \sigma_{ij}^{sgs}] = \dot{Q}_s$$

$$\frac{\partial \bar{\rho}\widetilde{Y}_m}{\partial t} + \frac{\partial}{\partial x_i}[\bar{\rho}\widetilde{Y}_m\widetilde{u}_i - \bar{\rho}\bar{D}_m\frac{\partial \widetilde{Y}_m}{\partial x_i} + \Phi_{i,m}^{sgs} + \theta_{i,m}^{sgs}] = \overline{\dot{w}}_m + \dot{S}_{s,m}$$

for m =1,N species.

Here, pressure is determined from the filtered equation of state, and $\overline{\tau}_{ij}$, the filtered viscous stress tensor and $\overline{q}_i$, the filtered heat conduction are approximated in terms of the filtered variables. The closure of the subgrid

*Graduate Research Assistant
†Professor

terms, such as, the stress tensor τ_{ij}^{sgs}, the heat flux H_i^{sgs}, the viscous work σ_i^{sgs}, the species mass flux $\Phi_{i,m}^{sgs}$, the diffusive mass flux $\theta_{i,m}^{sgs}$ and the filtered reaction rate $\overline{\dot{w}}_m$ are given elsewhere (Kim *et al.*, 1999).

The volume averaged inter-phase source terms that appear on the right hand side of the LES equations are given by (Pannala and Menon, 1998)

$$\begin{aligned}
\dot{\rho}_s &= [-\rho_d \frac{dV_d}{dt} + V_d \frac{d\rho_d}{dt}] \\
\dot{F}_{s,i} &= [(-\rho_d \frac{dV_d}{dt} + V_d \frac{d\rho_d}{dt}) u_{i,d} + \rho_d V_d \frac{du_{i,d}}{dt}] \\
\dot{Q}_s &= [(-\rho_d \frac{dV_d}{dt} + V_d \frac{d\rho_d}{dt}) e_{t,d} + \rho_d V_d \frac{de_{t,d}}{dt}] \\
\dot{S}_{s,m} &= [(-\rho_d \frac{dV_d}{dt} + V_d \frac{d\rho_d}{dt}) Y_{m,d} + \rho_d V_d \frac{dY_{m,d}}{dt}]
\end{aligned} \quad (1)$$

Here, ρ_d, V_d, $u_{i,d}$, $e_{t,d}$ and $Y_{m,d}$ are the density, volume, i-th component of the velocity, total energy and species mass fraction of the droplets, respectively. These terms are computed, as detailed elsewhere (Faeth, 1987).

Transport of Vaporizing Droplets

An Eulerian/Lagrangian approach, in which the droplets are tracked in a Lagrangian sense within an Eulerian gas field, is employed here. In this method, droplet groups (that represent droplets of same size, location, temperature and velocities) are tracked (instead of each droplet). The mass, momentum, energy and species transfer between the continuum and the dispersed phase is included at every time step. The gas phase LES velocity field and the subgrid kinetic energy are used to estimate the instantaneous gas velocity at the droplet location. A simple eight-point, volume-weighted averaging of the adjacent cells is used to interpolate the gas phase properties to the droplet locations and for the redistribution of the spray source terms from the particle position to the Eulerian grid. Drag effects due to the droplets on the gas phase is included using semi-empirical models (Faeth, 1987). To include stochastic dispersion of the droplets, a random velocity component is added to the gas phase fluctuating velocity. Heat transfer from gas phase to the liquid phase aids in the vaporization with the subsequent mass transfer to the gas phase. Thus, full coupling is achieved between the two phases in the present simulations.

Subgrid Momentum Closure

Here, the sub-grid stress tensor, τ_{ij}^{sgs}, is determined using the subgrid eddy viscosity which is obtained using the local grid size, $\overline{\Delta}$ and the sub-grid kinetic energy, k^{sgs}. The latter quantity is obtained by solving an equation for $k^{sgs} = \frac{1}{2}[\widetilde{u_k^2} - \tilde{u}_k^2]$ in the following form (Menon *et al.*, 1996):

$$\frac{\partial \overline{\rho} k^{sgs}}{\partial t} + \frac{\partial}{\partial x_i}(\overline{\rho}\tilde{u}_i k^{sgs}) = P^{sgs} - D^{sgs} + \frac{\partial}{\partial x_i}\left(\overline{\rho}\frac{\nu_t}{Pr_t}\frac{\partial k^{sgs}}{\partial x_i}\right) + F_k \quad (2)$$

Here, $Pr_t = 0.90$ is used, P^{sgs} and D^{sgs} are, respectively, the production and dissipation of subgrid kinetic energy. The production term, $P^{sgs} = -\tau_{ij}^{sgs}(\partial\tilde{u}_i/\partial x_j)$, where τ_{ij}^{sgs} is modeled using an eddy-viscosity which is given by, $\nu_t = C_\nu (k^{sgs})^{1/2}\overline{\Delta}$ and the dissipation term is modeled as $D^{sgs} = C_\varepsilon \overline{\rho}(k^{sgs})^{3/2}/\overline{\Delta}$. The coefficients, C_ν and C_ε are taken as constant at present (0.067 and 0.916, respectively), however, they can be dynamically determined locally (Kim *et al., 1999*).

In the above formulation, F_k represents the work done due to the two-phase coupling force term $\dot{F}_{s,i}$ and provides an additional coupling between the turbulent motion of the droplets and the evolution of the subgrid kinetic energy. Thus, k^{sgs} is indirectly modified due to particle drag and vaporization, since the force term $\dot{F}_{s,i}$ will change the resolved velocity field, which in turn will change the subgrid kinetic energy. This term is modelled as $F_k = < u_i \dot{F}_{s,i} > - \tilde{u}_i \dot{F}_{s,i}$ (Pannala and Menon, 1998).

Subgrid Scalar Closure

Two terms, the subgrid scalar flux, $\theta_{i,m}^{sgs} = \bar{\rho}[\widetilde{V_{i,m}Y_m} - \tilde{V}_{i,m}\tilde{Y}_m]$ and the filtered reaction rate term, $\overline{\dot{w}}_m$ require closure. In a conventional approach (used in Case C1, see below), a gradient approximation: $\theta_{i,m}^{sgs} \approx -\overline{\rho}\nu_t \nabla\tilde{Y}_m/Sc_m$, where Sc_m is a turbulent Schmidt number (assumed to be unity), is employed for the subgrid scalar flux. Note that, since large-scale motion is resolved in a LES, associated counter-gradient processes are resolved (even when a gradient closure is employed for $\theta_{i,m}^{sgs}$).

The closure for $\overline{\dot{w}}_m$ is complicated due to its highly non-linear nature. In the present study, an infinite rate chemistry is used which eliminates the need to model the reaction rate term.

However, the subgrid LEM method described below addresses this limitation in a more fundamental manner so that no closure is required for both $\theta_{i,m}^{sgs}$ and $\overline{\dot{w}}_m$.

In the LEM closure, the species field evolves within each LES cell due to localized, stochastic reaction-diffusion processes and are then transported across the LES cells due to convective flux. The local subgrid domain within each LES cell is resolved on a one-dimensional domain that resolves all scales of motion and thus, processes within this domain can be considered a localized 1D DNS (see Menon *et al.*, 1993; Chakravarthy and Menon, 2001). To describe this method, consider the "exact" reaction-diffusion equation for a scalar Φ

$$\frac{\partial \Phi}{\partial t} + (\tilde{u_i} + u_i^{'})\frac{\partial \Phi}{\partial x_i} = \frac{\partial}{\partial x_i}[D_\Phi \frac{\partial \Phi}{\partial x_i}] + \dot{\omega_\Phi} + \dot{S}_\Phi \tag{3}$$

Here, $\tilde{u_i}$ and $u_i^{'}$ are the resolved and unresolved velocities, respectively. Also, $u_i^{'}$ is due to both Lagrangian convection through the cell face $u_{lag}^{'}$, and turbulent convection at scales smaller than the resolved grid, $u_{stir}^{'}$. Both these terms are included in the LEM approach explicitly. Finally, $\dot{S}_\Phi$ is a non-zero source term only for the fuel species due to phase change from its liquid phase.

In the present methodology, a fractional splitting technique:

$$\frac{\Phi^* - \Phi^n}{\Delta t} = (\tilde{u_i} + u_{lag}^{'})\frac{\partial \Phi}{\partial x_i} \tag{4}$$

$$\Phi^{n+1} - \Phi^n =$$

$$\int_{t_o}^{t+\Delta t} [u_{stir}^{'}\frac{\partial \Phi}{\partial x_i} + \frac{\partial}{\partial x_i}(D\frac{\partial \Phi}{\partial x_i}) + \dot{\omega} + \dot{S}_\Phi]dt \tag{5}$$

is used to evolve the scalar field within the LES domain. Equation (4), which represents the advection of the scalar field by the resolved velocity field is modelled by a volume of fluid (VOF) approach (Chakravarthy and Menon, 2001) in which the LEM domains are convected across the cell face based on mass flux conservation. Equation (5) represents the subgrid reaction-diffusion processes that occur locally within each LES cell using the LEM model. Three processes occur within each LES cell: turbulent convection at scales smaller than the resolved grid (which is modelled using stochastic stirring events called triplet maps, see Menon *et al.*, 1993), molecular diffusion and finite-rate kinetics. Additional details are given in cited references.

NUMERICAL APPROACH

The LES equations are solved using a finite-volume scheme that is second-order accurate in space and time (a fourth-order spatially accurate scheme is also available for future studies). No-slip, adiabatic wall conditions conditions are used along with non-reflecting inflow/outflow boundary conditions. Clustering is employed near walls and in shear layers to better resolve large scale fluctuations. A computational grid of 141 x 75 x 81 is employed in all these simulations.

Two different configurations: one with a straight inlet pipe, expanding into a cylindrical combustor (C1 configuration) and a geometry which consists of a converging inlet section with a central injector cone (C2 configuration), are studied here. Figures 1a,b show, respectively, the geometries along with the computational grid. The inlet pipe simulates the region downstream of a swirler device. A swirl velocity profile (along with a turbulent fluctuating field of 7%) intensity is imposed at the inlet with a mean inlet mass flow rate of 0.435 Kg/sec at a temperature and pressure of 810 K, and 13.8 MPa, respectively. The Reynolds number based on inlet bulk velocity and inlet diameter is $\approx$ 370,000.

For Case C1, the droplets are injected at the centerline while for Case C2, the droplets are injected from the lateral sides of the central cone at an angle to the flow. Particle displacement is integrated using a fourth order Runge-Kutta method. Elastic wall collisions are assumed and a total of (approximately) 100,000 droplet groups are simulated. In the present study, particles of a constant size (20 microns) are injected (Stokes number is 8.2)and when they become smaller than 5 microns they are assumed to become fully vaporized. Earlier studies (Pannala and Menon, 1998) have demonstrated that this assumption is likely to be flawed since the final stage of vaporization can impact the mixing and combustion process. Future studies will address this issue further.

Inclusion of spray introduces new time scales in the flow. To accurately calculate the particle trajectories, size and temperature, the Lagrangian timestep used for the integration has to be the smallest of the time scales involved. The spray time step at any instant is determined as the minimum of the following timescales. droplet velocity relaxation time, droplet life time, droplet surface temperature constraint time, local grid time scale and tur-

bulent eddy droplet interaction time. The definitions and the expressions for calculating the various timesteps are given in Faeth (1987).

RESULTS AND DISCUSSION

Here, we summarize some of the key results obtained in the present study.

The C1 configuration

For the C1 configuration, three cases have been simulated. These are: a swirling, non-reacting case without droplets (unladen case), a swirling, non-reacting case with droplets and with momentum coupling (but with no vaporization), and a swirling, reacting spray (with infinite rate kinetics) case with full coupling.

General observation for these configurations show that the larger particles do not follow the gas phase due to their large inertia. But, as they get smaller due to vaporization, they equilibrate with the gas phase. Smaller droplets are observed (not shown, for brevity) in the recirculation bubble near the dump plane. On the other hand, in the momentum coupled (but without vaporization) case (also not shown), fewer particles are seen in the recirculation bubble because of the larger Stokes number for these (un-vaporized)particles.

Analysis of the flow features showed that the droplets tend to accumulate in regions of low vorticity. This type of preferential accumulation of droplets in regions of low vorticity was also observed in earlier studies of mixing layer (Pannala and Menon, 1998). The conditional expectation of droplet number density conditioned on vorticity is shown in Fig. 2. The abscissa in this plot is the normalized vorticity magnitude (normalized by the maximum vorticity in the whole domain). It can be observed that the PDF is non-symmetric, and is biased towards the low-vorticity side.

Figures 3(a) and (b) show respectively, the radial profiles (just slightly downstream of the dump plane) of the streamwise and transverse velocity profiles for the three cases. It can be seen that the peak values are significantly reduced due to the presence of droplets. The effect is even more pronounced when heat release is included. This reduction is due to momentum transfer between the gas and the liquid phases.

Figures 3(c) and (d) show respectively, the radial profiles of the velocity fluctuations in streamwise and transverse directions. Again, turbulent fluctuations have been significantly attenuated in the presence of the particles. Especially in regions of high turbulence, the effect of particles is more predominant. This is because in regions of high intensities the local Stokes number based on the turbulent time scales is high. This leads to increased attenuation of the turbulence (which occurs in the shear layer where turbulence production is very high). This result is consistent with the earlier study (Fessler, 1999). On the other hand, turbulence levels in the recirculating zone is not affected considerably, due to the presence of fewer particles there.

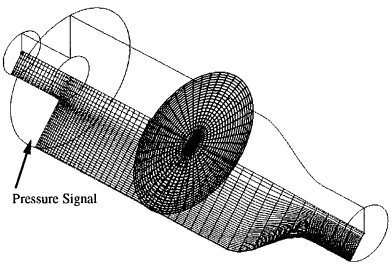

(a)

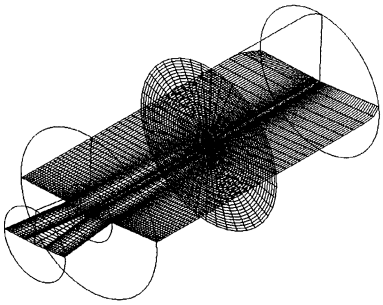

(b)

Figure 1: Two computational grid employed in this study.

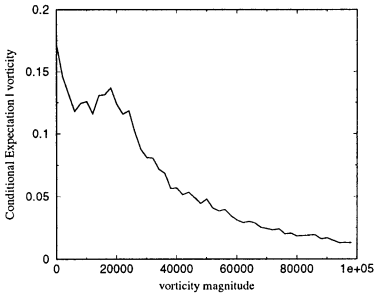

(a)

Figure 2: Conditional expectation of droplet number density.

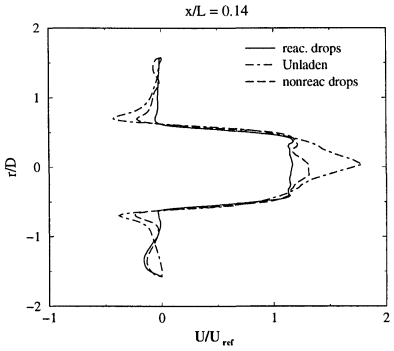

(a) Streamwise mean velocity

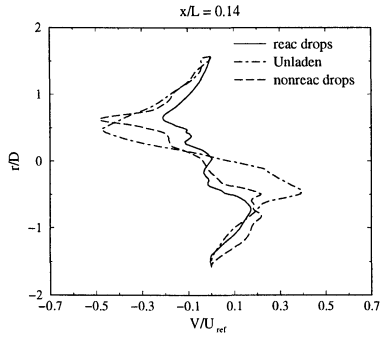

(b) Transverse mean velocity

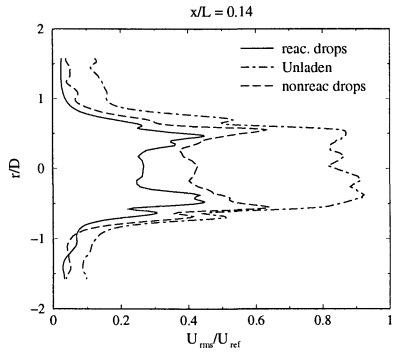

(c) Streamwise rms velocity

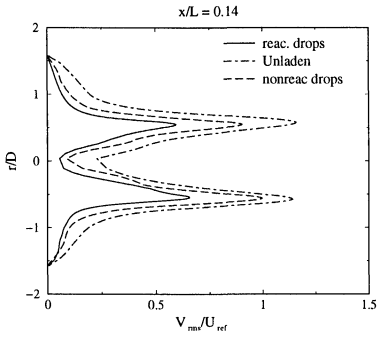

(d) Transverse rms velocity

Figure 3: Mean and rms radial velocity profiles for the C1 configuration at x/L = 0.14.

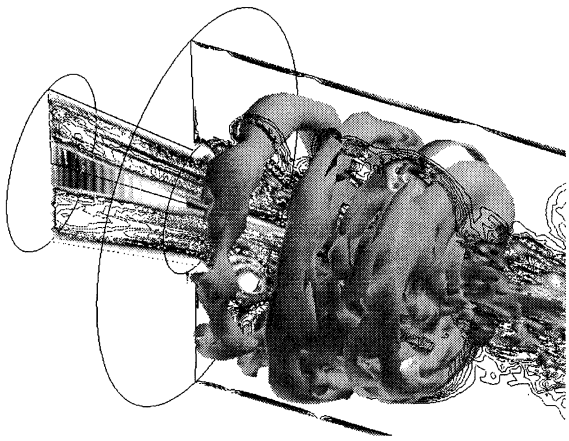

(a)

Figure 4: Crossplane instantaneous image of the vorticity magnitude and iso-surface of temperature showing the location of the flame.

The C2 configuration

For the C2 configuration, the liquid jet is injected through the central injector cone in the inlet. This type of injection impacts the spray transport and mixing process considerably. More detailed simulations of this configuration are underway and will be reported soon. Here, we summarize some key results obtained so far. Figure 4 shows the vorticity distribution in the cross plane and the iso-temperature surface marking the flame in the combustor. Formation and shedding of near-circular vortical rings from the inlet dump plane is clearly seen. Spray droplet transport is modulated by these rings but as the droplets evaporate, the gaseous fuel is entrained into the vortical regions where they mix with air and burn. This process is highly unsteady and dynamic and the current LES approach provides an unique capability to capture these phenomena.

Mean and rms velocity profiles of the gas phase in streamwise and spanwise directions for the C2 configuration are not much different from the C1 configuration (and therefore, not shown). Figure 5 shows the mean axial velocity decay along the center line of the combustor. Axial velocity decay seems to be highest for the unladen flows (for C1). The presence of particles seems to reduce the rate of axial velocity decay; however, more analysis is needed to understand this observation.

CONCLUSIONS

LES of two-phase reacting flows in a swirling gas turbine combustor has been carried out

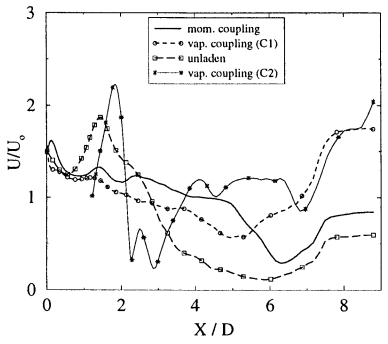

(a)

Figure 5: Centerline decay of the axial velocity

to understand the dynamics of the interaction between the two phases. The present model includes a more fundamental treatment of fuel-air mixing at the small-scales and allows incorporation of finite-rate kinetics without requiring ad hoc closure models. Global behavior of the spray combustion such as the preferential concentration of droplets, droplet dispersion and turbulence modification by the particles are all captured reasonably well by the present formulation. However, more work is still needed, especially to elucidate the effect of the mass loading ratio, droplet vaporization rate, and Stokes number on the combustion process.

ACKNOWLEDGMENTS

This work was supported in part by the Army Research Office (ARO) under the Multidisciplinary University Research Initiative (MURI). Computational time was provided by DOD High Performance Computing Centers at NAVO (MS), and ERDC (MS) under a ARO HPC Grand Challenge Projects.

References

Chakravarthy, V. and Menon, S., 2001, "Large-eddy simulations of turbulent premixed flames in the flamelet regime," *Combustion Science and Technology*, Vol. 162, pp. 1–48.

Faeth, G. M., 1987, "Mixing, transport and combustion in sprays," *Progress in Energy and Combustion Science*, Vol. 13, pp. 293–345.

Fessler, J. R. K., Eaton. J., 1999, "Turbulence modification by particles in a backward facing step flow", *Journal of Fluid Mechanics*, Vol. 394, pp. 97–117.

Kim, W.-W., Menon, S. and Mongia, H. C. 1999, "Large eddy simulations of a gas turbine combustor flow," *Combustion Science and Technology*, Vol. 143, pp. 25–62.

Menon, S. and Calhoon, W., 1996, "Subgrid mixing and molecular transport modeling for large-eddy simulations of turbulent reacting flows," *Proceedings of the Combustion Institute* Vol. 26, pp. 59–66.

Menon, S., McMurtry, P. and Kerstein, A. R., 1993, "A linear eddy mixing model for large eddy simulation of turbulent combustion," *in* B. Galperin and S. Orszag, eds, "LES of Complex Engineering and Geophysical Flows," Cambridge University Press, pp. 287-314.

Menon, S., Sankaran, V., Stone, C. and Sekar, B., 1999, "Dynamics of swirling premixed and spray flames," *AIAA-2001-1092.*

Menon, S., Yeung, P.-K. and Kim, W.-W., 1996, "Effect of subgrid models on the computed interscale energy transfer in isotropic turbulence," *Computers and Fluids*, Vol. 25, pp. 165–180.

Pannala, S. and Menon, S. 1998, "Large eddy simulations of two-phase turbulent flows," *AIAA 98-0163, 36th AIAA Aerospace Sciences Meeting.*